Available online at BCREC website: https://bcrec.id

Bulletin of Chemical Reaction Engineering & Catalysis, 18 (4) 2023, 713-723

Research Article

One-Step Hydrothermal Synthesis of TiO_2 Nanotubes and Photodegradation Activity towards Diazinon

Tanti Haryati*, Alvina Nur Diana, Ovy Sofiyah, Tusiana Putri Nelumbium, Novita Andarini, Yudi Aris Sulistiyo, S. Suwardiyanto

Department of Chemistry, Faculty of Mathematics and Natural Science, Jember University, Jember 68121, Indonesia.

Received: 16th October 2023; Revised: 28th November 2023; Accepted: 28th November 2023
Available online: 29th November 2023; Published regularly: December 2023

Abstract

The study aimed to analyze how variations in TiO_2/NaOH mole ratio, stirring time, and washing pH affect the formation process of TiO_2 nanotubes (TNT) through one-stage hydrothermal. TiO_2 micro powder was mixed with 10M NaOH with the variation of TiO_2/NaOH mole ratio (0.005:1, 0.015:1, and 0.025:1). The hydrothermal process was then conducted at 130 °C in an autoclave for 24 h with stirring time intervals of 10, 15, and 20 minutes/h. The samples underwent 1 M HCl washing to produce diverse pH variations (pH = 2, pH = 3, and pH = 4). Characterization of the synthesized TNT was conducted using Scanning Electron Microscope (SEM), Transmission Electron Microscope (TEM), X-ray Diffraction (XRD), Surface Area Analyzer (SAA), and Ultra Violet Visible Diffuse Reflectance Spectroscopy (UV-Vis DRS). After analysis of the micrographs revealed the fiber shape of the particles, it was noted that TNT particle size increased due to smaller mole ratio variation, longer stirring, and lower pH. The synthesized TNT featured a tubular morphology with an inner diameter of 3.30 nm, an outer diameter of 6.15 nm, and a wall thickness of 1.64 nm. The increase in sodium titanate content of the sample results in an increase in surface area. Additionally, small pore size contributes towards an increase in both surface area and total pore size. The best result of the TNT photocatalytic test against diazinon can be observed in the fifth sample with a mole ratio of 0.025:1, stirring time of 20 minutes/h, and washing pH of 3. With an irradiation time of 210 min, diazinon degradation reached 90%.

Keywords: TiO_2 Nanotubes (TNT); Stirring Time; Mole Ratio; Washing pH; Photodegradation; Diazinon

How to Cite: T. Haryati, A.N. Diana, O. Sofiyah, T.P. Nelumbium, N. Andarini, Y.A. Sulistiyo, S. Suwardiyanto (2023). One-Step Hydrothermal Synthesis of TiO_2 Nanotubes and Photodegradation Activity towards Diazinon. *Bulletin of Chemical Reaction Engineering & Catalysis*, 18(4), 713-723 (doi: 10.9767/bcrec.20056)

Permalink/DOI: https://doi.org/10.9767/bcrec.20056

1. Introduction

Titanium dioxide (TiO_2) possessing an anatase crystal phase is a semiconductor material that exhibits promising photocatalysis activity [1]. The photocatalytic activity of TiO_2 can be improved by changing the particle size to nanosize, thus increasing the surface area [2]. Various morphologies of TiO_2 nanomaterials have been prepared, including nanofibers, nanowires, nanorods, nanotubes, and nanosheets [3]. Nanotubes exhibit a tube-shaped morphology with an elongated structure and an inside cavity [4].

The synthesis of TiO_2 nanotubes (TNT) can be achieved through different methods such as hydrothermal, sol-gel, and anodization. The hydrothermal method is a chemical process that employs water solvents or mineralizers at high temperatures and pressures in a closed system [5]. Various factors, including mole ratio [6],

* Corresponding Author.
Email: tanti@unej.ac.id (T. Haryati)

stirring time, hydrothermal time [7], and pH [8], may affect the formation of TNT material by the hydrothermal method. The study by Shahrezaei *et al.* [9] investigated TNT synthesis by varying the mole ratio of TiO_2/NaOH and found that a smaller ratio led to a higher surface area production. Sallem *et al.* [7] conducted TNT synthesis using a one-stage hydrothermal method by varying the stirring time. Homogeneous mixing of particles in an autoclave through stirring resulted in uniform morphology. Longer stirring, however, can cause an increase in particle size. The addition of hydrochloric acid to a range of 1-3 during washing may lead to the formation of TNT with a diameter of 10-30 nm and a surface area of approximately 100-300 m^2/g [10].

TNT can act as a photocatalyst to break down diazinon pollutants that are insoluble in water. Exposure to light stimulates the excitation of electrons, leading to the creation of electron holes and the formation of (•OH) radicals. These (•OH) radicals can be deployed for the degradation of organic pollutants [11]. The degradation of diazinon compounds may be affected by the duration of irradiation. Lengthier exposure to radiation leads to increased degradation percentage due to the interplay between the photocatalyst and longer photon energy [12].

This study investigates the synthesis of TNT through a one-stage hydrothermal technique that employs variations in mole ratio, stirring, and washing pH. The study further evaluates the effectiveness of synthesized TNT for photodegradation of diazinon. The objective of this investigation is to analyze the effects that the three different variables have on the TNT characteristics and its ability for diazinon photodegradation.

2. Materials and Methods

2.1 Materials

The materials used in this experiment were NaOH solids (Merck), distilled water, HCl 37%, TiO_2 micro powder (Merck), NaH_2PO_4 (Merck), Na_2HPO_4 (Merck), aluminum foil, commercial Diazinon 600 EC (PT. Petrokimia Kayaku), cooking oil, universal pH paper, and Whatman 42 filter paper.

2.2 Synthesis of TiO_2 Nanotubes (TNT)

TNT was synthesized via a single-stage hydrothermal technique. TiO_2 micro powder, serving as a precursor, was dissolved in 85 mL of 10 M NaOH at the rates of 0.339, 1.017, and 1.697 grams. The mixture was stirred at 300 rpm for 30 min and then transferred into a 100 mL autoclave. The autoclave was sealed tightly and put into an oil bath covered with aluminum foil for the hydrothermal process. The hydrothermal process took place at a temperature of 130 ℃ for a duration of 24 h [7], with diverse stirring times of 10, 15, and 20 minutes/h (400 rpm); these are illustrated in Table 1. Stirring commenced at the beginning of each hour, with a definite stopping time, before continuing in the following hour, until the completion of the hydrothermal time. The autoclave was cooled for 3 hours at room temperature. The solid materials were placed into a glass beaker and washed gradually with a 1 M HCl solution. While being stirred using a magnetic stirrer, the solution achieved varying pH levels of pH = 2, pH = 3, and pH = 4 [8]. After decanting, the contents were washed again with distilled water to neutralize the pH level and then filtered. The solid material was dried in an oven at 80 ℃ for 12 h and calcined at 400 ℃ for 2 h. The produced TNT was then analyzed using SEM, TEM, XRD, SAA, and UV-Vis DRS spectrophotometer. Table 1. Variation of TNT Synthesis from TiO_2 micro powder.

2.3 Characterizations

The samples' surface was analyzed utilizing the SEM (JEOL JSM-IT 200) and particle size was computed utilizing the ImageJ software. The surface area, pore size, and pore volume of TNT were evaluated by employing the Quantachrome Nova 4200e. The surface area data was obtained through the application of the BET Multi-point method, while the pore volume was determined by the BJH Pore Size

Table 1. Variation of TNT Synthesis from TiO_2 micro powder.

Samples	Mole Ratio of TiO_2/NaOH	Stirring Time (minutes/hour)	Washing pH
1	0.005:1	10	3
2	0.015:1	10	3
3	0.025:1	10	3
4	0.025:1	15	3
5	0.025:1	20	3
6	0.025:1	10	2
7	0.025:1	10	4

Distribution Desorption method, through adsorption-desorption of N_2 gas at temperatures of 77.35 K and P/P_0 range of 0.1-1.0. The nanotube morphology of TNT was observed via images acquired by TEM (JEM-1400), and its diameter was measured using ImageJ software. XRD (Xpert MPD PANalytical) was employed to characterize the diffraction patterns of TNT with a range of 5-60° at 2θ. Reflectance data recorded with a UV-Vis DRS Spectrophotometer (Shimadzu-2450) within the wavelength range of 200-800 nm were used to carry out measurements of band gap energy. Measurement of the concentration of diazinon was conducted by analyzing absorbance data captured by a UV-Vis Spectrophotometer (Thermo Scientific Genesys 10S UV-Vis) over a range of wavelengths between 200 and 400 nm.

2.4 Determination of Photocatalytic Activity

The photocatalytic activity of TNT on organic pollutants of the diazinon compound was conducted in a box-shaped photocatalytic reactor covered with aluminum foil. The light used is an ultraviolet lamp (Philips Stick 40 W lamp). Solution diazinon 25 ppm as much as 20 mL and TNT each variation as much as 50 mg put into a glass beaker 50 mL. The irradiation process is carried out at room temperature (25 °C) and the pH of the solution is 7. The beaker glass filled with the mixture is included in the photoreactor. The degradation process was accompanied by constant stirring (300 rpm) with 30, 120, and 210 minutes of irradiation. The photodegradation results were centrifuged at 3000 rpm for 30 minutes and allowed to stand until two phases were formed. The solution was separated using filter paper to obtain filtrate and residue. The filtrate obtained was analyzed using a UV-Vis spectrophotometer in the wavelength range of 200-400 nm.

2.5 Analysis of Photodegradation

The photodegradation test results were analyzed using the calibration curve equation, which was created with diazinon standard solution concentrations ranging from 1 ppm to 25 ppm. The absorbance results were measured in the maximum wavelength region. To calculate the concentration of degraded diazinon, the line equation, $y = mx + c$, was used, with variable x representing the concentration of photodegraded diazinon (C_t).

$$C_t = \frac{y - c}{m} \quad (1)$$

The percentage of diazinon degradation (R(%)) was calculated using Equation (2).

$$R(\%) = \frac{C_0 - C_t}{C_0} \times 100\% \quad (2)$$

3. Results and Discussions

3.1 Morphology and Particle Size of TNT

The morphology and particle size of TNT were determined through observations on Scanning Electron Microscope (SEM) images. TNT was synthesized using a TiO_2 micropowder precursor, characterized by a spherical particle shape with an average size of 194.29 nm. Figure 1(a) illustrates the original spherical particle shape, which was transformed into fibers as shown in Figure 1(b-d). The results of TNT synthesis by the hydrothermal method were obtained. This suggests that the hydrothermal process can disintegrate micro-sized TiO_2 particles and reorganize them into sheet form, leading to their rolling and ultimately forming fibers.

The micrographs in Figure 1 depict TNT samples 1, 2, and 3 with varied TiO_2/NaOH mole ratios. The decrease in mole ratio of TiO_2/NaOH leads to an increase in the average particle size of TNT. Samples 1, 2, and 3 resulted in average particle size measurements of 49.08, 40.20, and 26.43 nm. This phenomenon arises from the greater presence of NaOH during the hydrothermal process as the mole ratio decreases. In the synthesis of TNT, the reaction between TiO_2 micro powder and NaOH enables the production of sodium titanate with a lepidocrocite-type structure through a complex process [13]. The presence of Na^+ in NaOH disrupts the Ti−O−Ti bond with a bond energy of 667±7 kJ/mol. This allows Na^+ to penetrate the TiO_2 micro powder structure and form a new Ti−O−Na bond. The reaction causes the creation of intermediate phases, leading to the generation of lamellar fragments during the building of nanotube structures [14].

NaOH acts as a mineralizer, influencing both crystal growth and core formation processes. As the quantity of Na^+ ions increases, the solubility rate of TiO_2 micro powder and the rate of formation of sodium titanate also increase. As a result, the solution reaches its super-saturated state at a faster speed and the nucleation rate reaches its maximum concentration at a faster rate. The speed of crystal nucleus formation surpasses that of crystal growth, leading to the formation of small TiO_2 crystals [15]. The mole ratio of TiO_2/NaOH in-

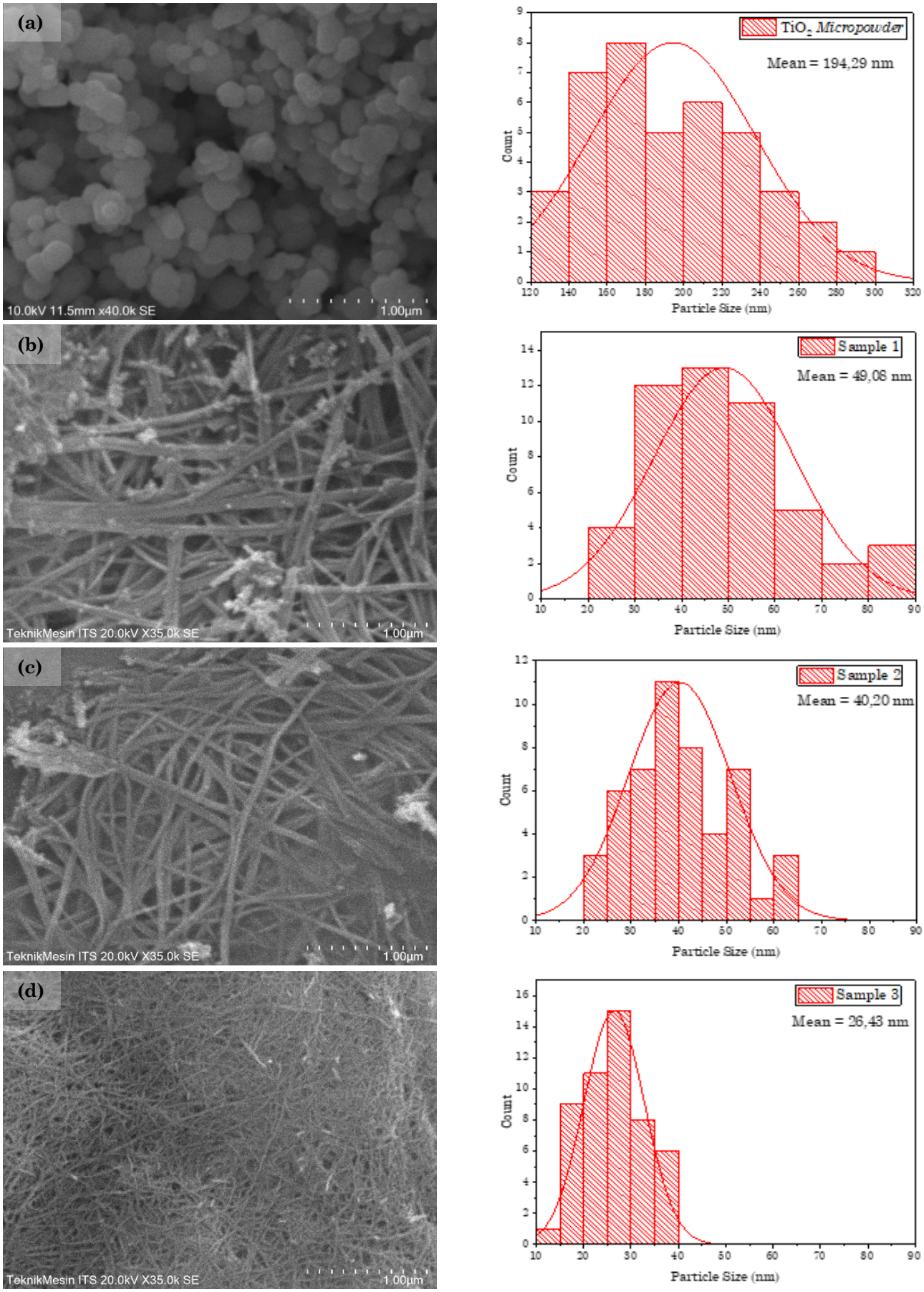

Figure 1. SEM results and Particle Size Distribution (a) TiO_2 micro powder, (b) Sample 1, (c) Sample 2, (d) Sample 3.

fluences TNT particle size, with smaller ratios resulting in larger particles. This is because the crystal nuclei formed in sample 1, which has the smallest mole ratio, are fewer than those in samples 2 and 3. Upon completion of the hydrothermal process, the superheated conditions decrease during the cooling process, allowing for crystal nuclei to interact and develop into larger crystals.

The effective synthesis of TNT is also affected by the duration of stirring time as presented in Figure 2. The micrograph outcomes of sample 3, sample 4, and sample 5, with prolonged stirring periods, led to a more extensive range of TNT particle sizes being produced. This phenomenon may be attributed to the ease of particle dissolution due to constant stirring, leading to the formation of fewer crystal nuclei.

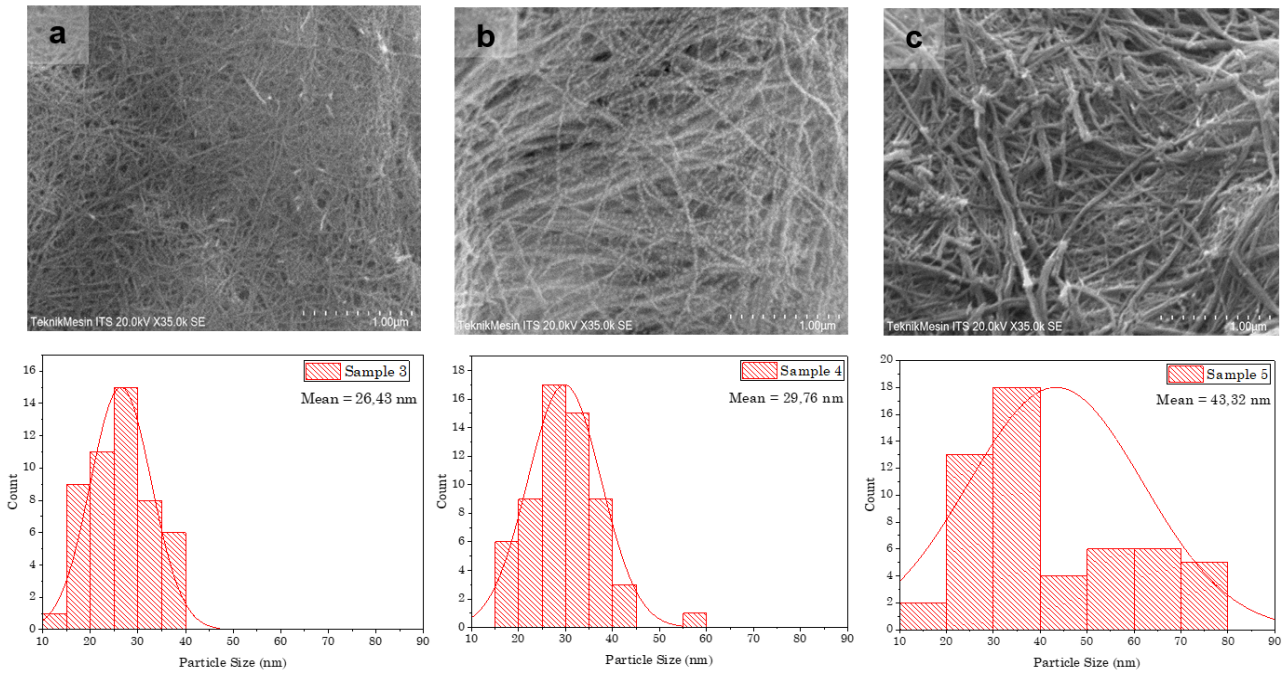

Figure 2. SEM results and Particle Size Distribution (a) Sample 3, (b) Sample 4, (c) Sample 5.

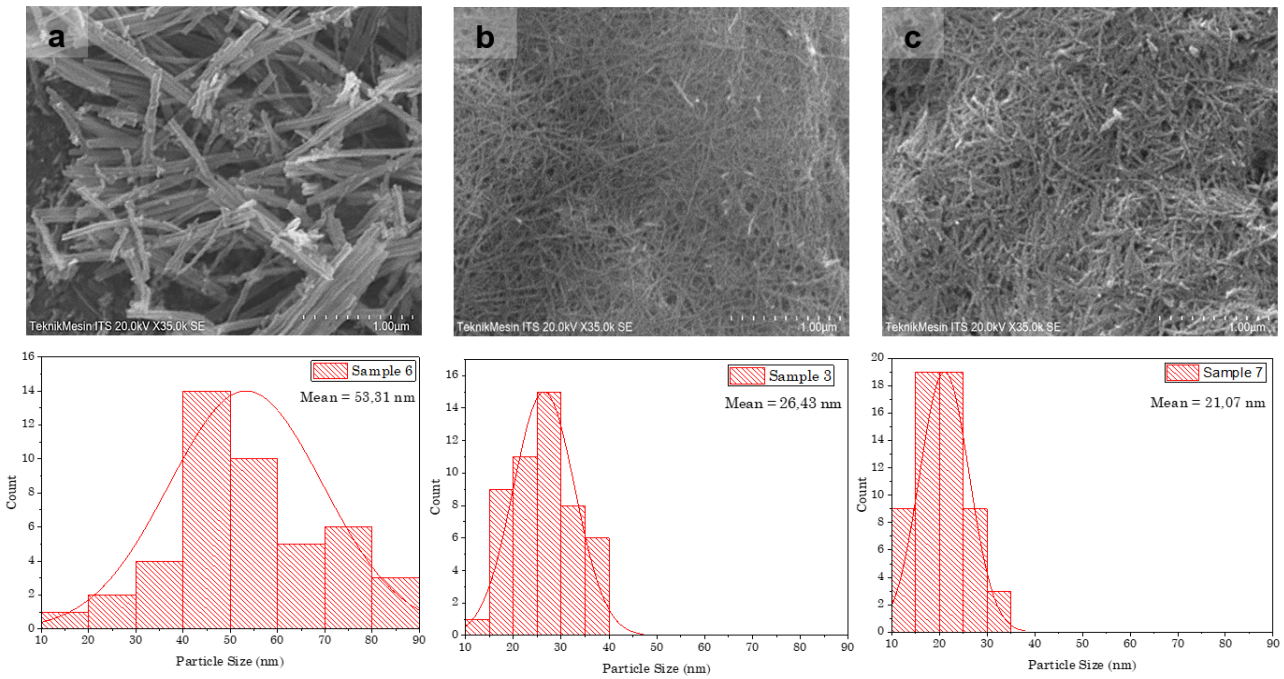

Figure 3. SEM results and particle size distribution (a) Sample 6 (pH = 2), (b) Sample 3 (pH = 3), (c) Sample 7 (pH = 4).

High solubility, as explained by Xu *et al.* [16], accelerates the rate of crystal formation compared to that of crystal nucleation, leading to larger crystal sizes. The average particle sizes measured in samples 3, 4, and 5 were 26.43 nm, 29.76 nm, and 43.32 nm, respectively.

Figure 3 shows the micrograph of samples 3, 6, and 7, which underwent various post-hydrothermal pH levels in the presence of added HCl. The addition of acid results in the replacement of Na^+ ions present in the lamellar structure with H^+ ions, causing them to roll up and form a titanate hydrogen compound [8]. The highest TNT was achieved when the washing pH was low. The mean particle sizes (tube diameters) of samples 6, 3, and 7 are 53.31, 26.43 and 21.07 nm, respectively. A rise in pH levels causes a deceleration of molecular interactions, which, in turn, fosters the generation of crystal nuclei and a slower crystal growth process. Accordingly, a smaller particle size ensues [17].

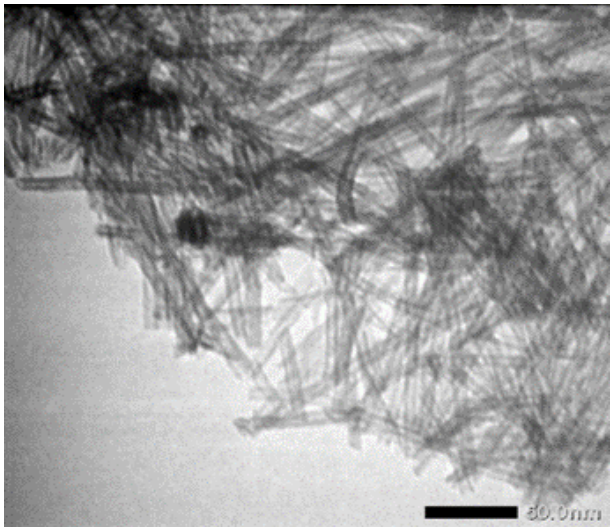

Figure 4. TEM characterization results of TiO_2 nanotubes in Sample 3.

Nanotube morphology was successfully formed in the synthesized TNT, as confirmed by TEM analysis of sample 3. Figure 4 illustrates the morphology in the form of an elongated tube. This study yielded an average outer diameter, inner diameter, and wall thickness of 6.15 nm, 3.30 nm, and 1.64 nm, respectively. Zulfiqar *et al.* [18] had previously reported that TNT possesses an outer and inner diameter of 4-10 nm and 2-3 nm, respectively.

Elemental composition analysis of TNT in sample 3 was conducted via EDX analysis. Figure 5 displays the EDX spectrum, revealing that TNT composition comprises 85% Ti element, 11% O element, and 4% Na element. The findings suggest that impurities persist in the form of sodium titanate. As per Liu *et al.* [19], sodium titanate is challenging to dissolve with NaOH, resulting in complicated nanotube formation.

3.2 TNT Crystalline Phases

The crystallinity and crystalline phase of the synthesized TNT were determined through X-ray diffraction (XRD). Abbreviations will be explained when first used. The results, presented in Figure 6, include samples 1, 2, and 4, which reveal a diffraction pattern like JCPDS TiO_2 anatase. Sample 1 and sample 2 depict diffraction patterns displaying an anatase crystal phase at 2θ = 25.27°, 37.77°, 48.01°, 53.86°, and 55.01°. Sample 4 displays diffraction patterns of the anatase crystal phase at 2θ = 25.26°, 37.77°, 48.05°, 53.81°, and 55.07°. Anatase diffraction patterns at 2θ = 25.20°, 37.78°, 47.91°, 53.73°, and 54.84° are observed in Sample 6. The diffractograms attained in samples 3, 5, and 7 present impurities in the form of so-

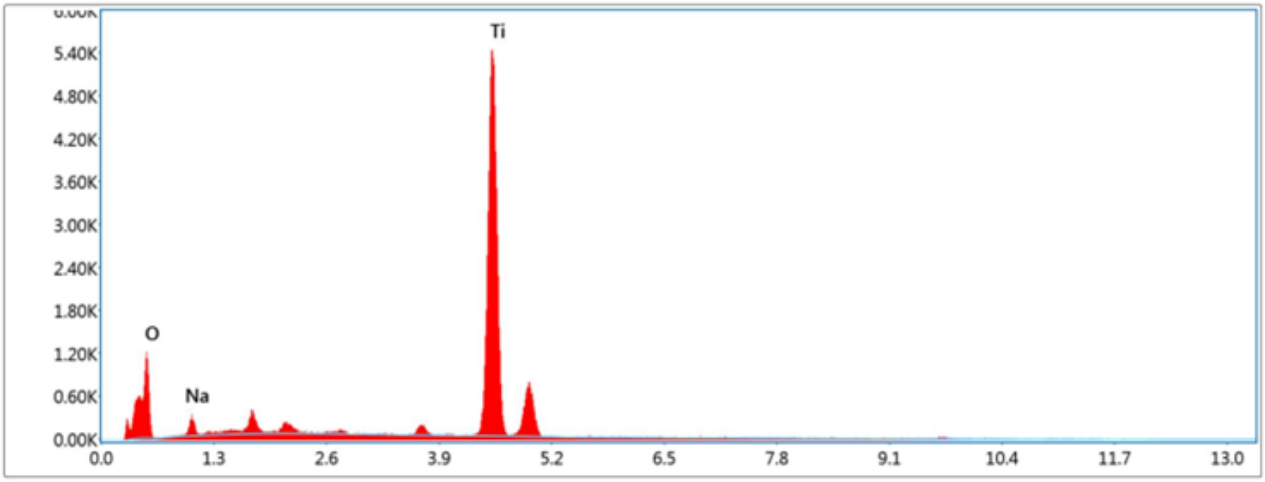

Figure 5. EDX Spectrum Results of Sample 3.

dium titanate. The reason for the sodium titanate content is the insufficiency in the washing process using HCl, which results in considerable Na^+ ions remaining in the sample.

Figure 6 demonstrates that samples 3, 5, and 7 display decreased crystallinity owing to the presence of sodium titanate within the samples. This can be attributed to the formation of stable crystalline sodium titanate, which infiltrates the pore structure of the nanotubes and becomes challenging to extract even with distilled water washing. Lee *et al.* [20] have suggested that sodium titanate or residual sodium ions occur in TNT samples because of the crystal formation process. The sodium titanate entrapped within the TNT pore forms a rolled-up layer, posing difficulties during the extraction process. Sodium's presence within the TNT pore configuration impairs the resulting diffraction pattern, leading to low crystallinity and a broader peak [8].

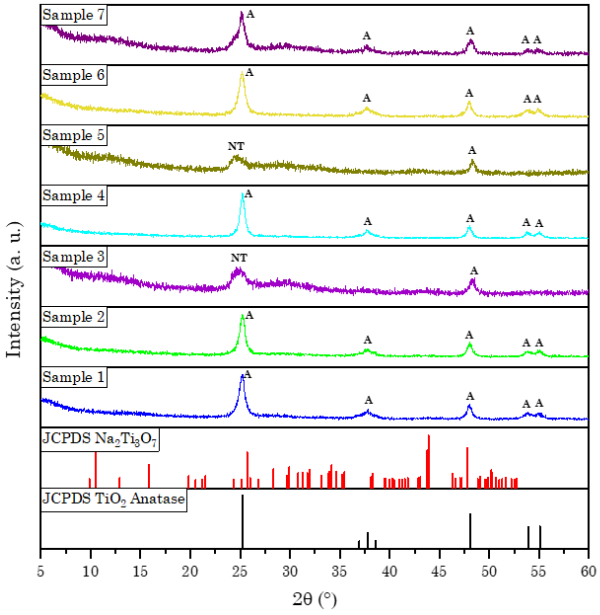

Figure 6. XRD diffractograms of TNT (A = Anatase and NT = Sodium Titanate).

3.3 TNT Surface Area and Pore Size

Surface area, pore volume, and pore size were characterized using the N_2 gas adsorption-desorption isotherm method. Section and citation formatting conforms to academic conventions. Unnecessary wording has been removed while maintaining a clear and logical flow of information. Passive voice and a formal register have been adopted. The isotherm model in Figure 7 exhibits a similar pattern to the IUPAC type IV(a) model, which is typical for mesoporous materials. The isotherm model in Figure 7 exhibits a similar pattern to the IUPAC type IV(a) model, which is typical for mesoporous materials. Technical terms are explained upon first use. The presence of narrow surface pores and wide interconnected inner pores is demonstrated by the H2(b) hysteresis loop, which leads to capillary condensation in the surface mesopores of the material [16]. Blockages during desorption can occur due to pore narrowing at the end of tubes in the shape of nanotubes. Hysteresis loops are observed in sample 1, sample 2, and sample 4 when the pressures (P/P_0) exceed 0.7, thereby indicating the presence of macropores in addition to meso-

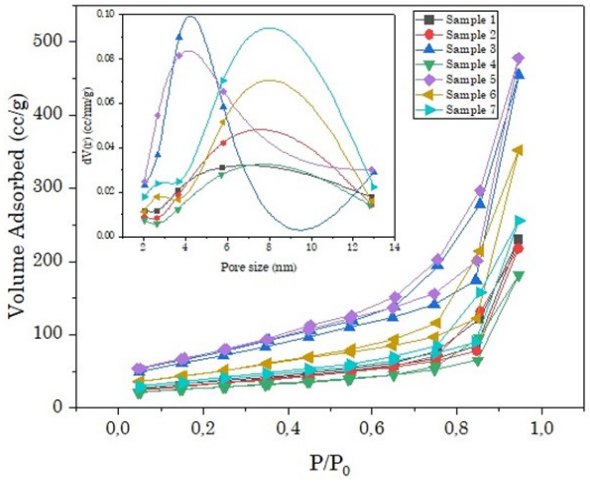

Figure 7. Adsorption-Desorption Isotherms of N_2 Gas of TNT Sample.

Table 2. Surface area and textural properties of TiO_2 Nanotubes.

Samples	Surface Area (m^2/g)	Average pore size (nm)	Pore Total Volume (cc/g)
TiO_2 Micro powder	1.58	-	-
Sample 1	115.491	6.179	0.357
Sample 2	109.942	6.150	0.338
Sample 3	241.142	5.848	0.705
Sample 4	91.198	5.724	0.282
Sample 5	266.038	3.702	0.741
Sample 6	128.306	6.176	0.396
Sample 7	171.219	6.386	0.546

pores [2]. The presence of cavities between TNT fibers may create macropores in the three samples. Analysis of SEM results in Sample 4 (Figure 2) and Samples 1 and 2 (Figure 1) reveal the presence of wider voids between fibers, while tighter fiber arrangements are seen in SEM images of other samples.

Table 2 displays the surface area results, indicating that surface area measurements for all six TNT samples, except for sample 4, fell within the specific TNT surface area range of 100-400 m^2/g [22]. As shown by the data, a greater mole ratio of TiO_2/NaOH results in a larger surface area. Sodium titanate impurities were responsible for the larger surface area in sample 3 (which had the largest mole ratio). According to Preda *et al.* [23], a greater sodium titanate concentration within the sample will result in a bigger surface area.

The surface area data of TNT is proportional to its pore volume data in seven TNT samples. Pore volume is an indicator of the nanotubes' pores or voids, as well as the voids or spacing between nanotube particles. The particle spacing in sample 1 is tighter than in sample 2. Consequently, the specific surface area in sample 2 is lower than that in sample 1. However, there is not a significant difference in surface area and pore volume between the two samples. The pore size measurements for the three TNT samples are equivalent to the particle size measurements of TNT. A greater pore size may result in a larger particle size (fiber diameter).

The duration of the stirring process has an impact on the surface area, pore size, and pore volume of TNT. It was found that when the sodium titanate content in the sample increased, the surface area of TNT also increased [22].

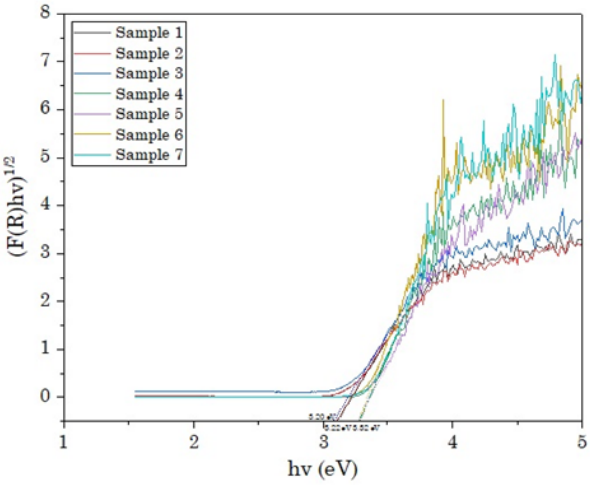

Figure 8. Graph of Kubelka-Munk relationship versus photon energy (hv).

The growth in total pore volume is consistent with the expansion in surface area. This is possible because lengthier stirring enlarges the cavity in the structure of TNT tubes. The elongation of the pores (cavities) leads to an increase in the volume of adsorbed N_2 gas, resulting in a greater surface area and total pore volume, as reported in [24].

The process of acid washing during post-hydrothermal treatment impacted the surface area, pore size, and pore volume of TNT. Viet *et al.* [23] conducted a synthesis of TNT at pH = 2, yielding a surface area of 83.5 m^2/g. In the case of sample 6, a surface area of 128.306 m^2/g was achieved. The observed outcome yielded a greater surface area in comparison to the research results of Viet *et al.* [8]. Meanwhile, according to the pore size (Table 2), sample 3 exhibited a smaller average pore size compared to sample 6 and sample 7. The pore size distribution of the seven TNT samples presented in Table 2 indicates that the TNT pore size falls within the mesopore range (2-50 nm) [14]. The pore analysis results based on SAA reveal conformity with the analysis based on TEM in sample 3.

3.4 TNT Band Gap Energies

The determination of band gap energy in the synthesized TNT samples can be done by employing a UV-Vis Diffuse Reflectance spectrophotometer (DRS). The Tauc Plot method is used to measure the band gap energy, and this method connects the photon energy value (hv) with the Kubelka-Munk function ($(F(R)hv)^n$). The transition that occurs is an indirect transi-

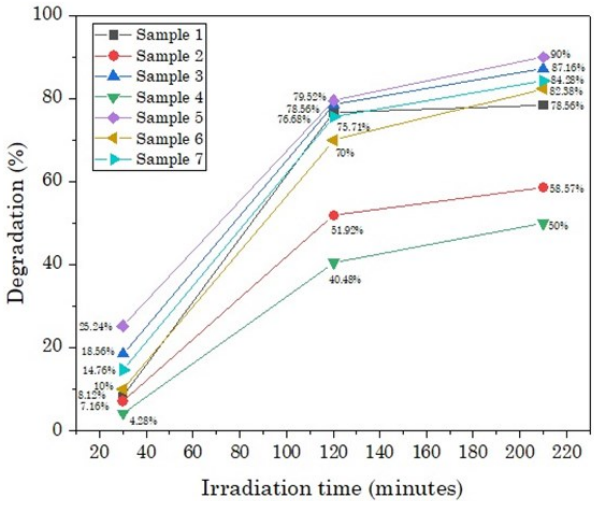

Figure 9. Graph of irradiation time versus percent degradation of diazinon. Diazinon = 25 mg/L (25 ppm), TNT = 50 mg, room temperature, pH = 7.

tion, with an n value of ½. According to Zhang and Dong [25], TiO_2 rutile is a direct transition semiconductor, while TiO_2 anatase is an indirect transition semiconductor.

The band gap energy values of samples 1 to 7 (Figure 8) are 3.22 eV, 3.22 eV, 3.20 eV, 3.32 eV, 3.32 eV, 3.32 eV, and 3.32 eV, respectively. Stirring has the potential to cause a diffusion of ions in the lattice and produce a new sub-gap energy, resulting in a band gap shift and increased band gap energy [20]. In sample 3, the presence of sodium titanate has caused a reduction in band gap energy. The existence of sodium in TNT may instigate intra-band transitions in energy-depleted regions. Unal *et al.* [26] reported that the value of band gap energy for anatase TiO_2 fluctuates between 3.20 and 3.40 eV in every experiment. Modifying the mole ratio, stirring time, and washing pH during post-hydrothermal did not notably influence the TNT band gap energy value alteration.

3.5 TNT Photocatalytic Effectiveness

The findings of the diazinon photodegradation experiment conducted by TNT are depicted in Figure 9. This figure is based on the correlation between the changes in irradiation duration and the reduction rate of diazinon. The experimental conditions involved the utilization of three irradiation durations 30, 120, and 210 minutes. Upon analysis of Figure 9, it can be inferred that specimen 5 displays robust photocatalytic efficacy, recording a 90% removal rate at 210 minutes of irradiation. The degradation capacity of diazinon may be affected by the specific surface area of TNT. A larger surface area leads to a higher percentage of degradation, as the greater surface area provides more active sites [27]. Another key factor that can enhance the efficacy of diazinon degradation by TNT is the length of irradiation time. As demonstrated in Figure 9, elongated irradiation time results in a greater extent of diazinon degradation. This phenomenon arises due to an elevated concentration of OH radicals (•OH), triggered by the prolonged time of irradiation.

The efficiency of diazinon photocatalyst can be boosted by 13% by incorporating TNT when compared to diazinon photocatalyst lacking TNT [11]. The process of photocatalysis cannot occur without UV light, hence diazinon cannot be degraded [28]. As TiO_2 material is a semiconductor, it requires more energy for the excitation of electrons to create electron and proton holes. Proton holes in the valence band oxidize H_2O, resulting in the formation of •OH. •OH radicals have an oxidation potential of 2.80 eV, which can then degrade organic pollutants into more environmentally friendly compounds [10]. UV light is deemed more reproducible and possesses higher energy than the band gap energy of TiO_2, resulting in increased efficiency of the degradation process compared to sunlight energy [29].

4. Conclusions

The study found that adjusting the mole ratio of TiO_2/NaOH, lengthening the stirring time, and altering the pH of post-hydrothermal washing has an impact on the physical and chemical characteristics of the samples. This, in turn, affects the morphology, textural properties, and band gap energy of the TNT synthesized. Furthermore, the ability of TNT to degrade diazinon compounds under ultraviolet light has been scientifically proven, with the percentage of diazinon degradation increasing proportionally to the irradiation time. The most successful photocatalysis outcomes were observed for sample 5 following 210 minutes of irradiation which resulted in a superior degradation percentage of 90%. Another influential factor impacting photodegradation activity is the specific surface area of TNT. The greater the TNT surface area, the greater the number of active sites, which leads to an increased percentage of degradation.

Acknowledgment

The author would like to thank the University of Jember which provided funding through "*Hibah Keris"* in the fiscal year 2022 for supporting the finances of the research.

CRediT Author Statement

Author Contributions: *T. Haryati*: Conceptualization, Methodology, Investigation, Resources, Data Curation, Writing, Review and Editing, Supervision; *A. N. Diana*: Methodology, Formal Analysis, Data Curation, Writing Original Draft Preparation, Visualization; *T. P. Nelumbium*: Methodology, Formal Analysis, Data Curation, Writting Original Draft Preparation, Visualization; *N. Andarini*: Resources, Visualisation, Review and Editing, Data Curation; Project Administration; *Y. A. Sulistiyo*: Formal Analysis, Review and Editing, Data Curation; *S. Suwardiyanto*: Formal Analysis, Review and Editing, Data Curation. All authors have read and agreed to the published version of the manuscript.

References

[1] Rajendran, R., Vignesh, S., Sasireka, A., Suganthi, S., Raj, V., Baskaran, P., Shkir, M., Alfaify, S. (2021). Designing Ag_2O Modified g-C_3N_4/TiO_2 Ternary Nanocomposites for Photocatalytic Organic Pollutants Degradation Performance Under Visible Light: Synergistic Mechanism Insight. *Colloids and Surfaces A: Physicochemical and Engineering Aspect,* 629, 1-13. DOI: 10.1016/j.colsurfa.2021.127472.

[2] Zhai, X., Yang, X., Liu, X., Dong, Y., Zhang, W. (2023). Sensitive Photocatalytic Reduction of High Concentration Chromium-Containing Wastewater Driven by One-Step Hydrothermal Synthesis of Bi-Element Modified TiO_2. *Applied Surface Science*, 622, 156976. DOI: 10.1016/j.apsusc.2023.156976.

[3] Chen, J., Ma, J., Fan, Q., Zhang, W. (2023). An Eco-Friendly Metalless Tanning Process: Zr-Based Metal-Organic Frameworks as Novel Chrome-Free Tanning Agent. *Journal of Cleaner Production*, 382, 135263. DOI: 10.1016/j.jclepro.2022.135263.

[4] Guo, R., Bao, Y., Kang, Q., Liu, C., Zhang, W., Zhu, Q. (2022). Solvent-Controlled Synthesis and Photocatalytic Activity of Hollow TiO_2 Microspheres Prepared by The Solvothermal Method. *Colloids and Surfaces A: Physicochemical and Engineering Aspect,* 633, 181-188. DOI: 10.1016/j.colsurfa.2021.127931.

[5] Byrappa, K., Yoshimura, M. (2013). *Handbook of Hydrothermal Technology Edition 2*. USA : William Andrew.

[6] Peng, T., Zhang, J., Ray, S., Saadat Ghareh Bagh, F., Fakhouri, H., Arefi-Khonsari, F., Lalman, J.A. (2019). Optimizing one-dimensional TiO_2 for photocatalytic hydrogen production from a water-ethanol mixture and other electron donors. *Journal of Environmental Chemical Engineering*, 7(1), 102868. DOI: 10.1016/j.jece.2018.102868.

[7] Sallem, F., Chassagnon, R., Megriche, A., El Maaoui, M., Millot, N. (2017). Effect of Mechanical Stirring and Temperature on Dynamic Hydrothermal Synthesis of Titanate Nanotubes. *Journal of Alloys and Compounds*, 722, 785–796. DOI: 10.1016/j.jallcom.2017.06.172.

[8] Viet, P., Phan, B.T., Van Hieu, L., Thi, C.M. (2015). The Effect of Acid Treatment and Reactive Temperature on The Formation of TiO_2 Nanotubes. *Journal of Nanoscience and Nanotechnology*, 15 (7), 5202–5206. DOI: 10.1016/j.spmi.2018.09.035.

[9] Shahrezaei, M., Habibzadeh, S., Babaluo, A. A., Hosseinkhani, H., Haghighi, M., Hasanzadeh, A., Tahmasebpour, R. (2017). Study of synthesis parameters and photocatalytic activity of TiO_2 nanostructures. *Journal of Experimental Nanoscience*, 12 (1), 45–61. DOI: 10.1080/17458080.2016.1258495.

[10] Lee, C.K., Wang, C.C., Lyu, M.D., Juang, L.C., Liu, S.S., Hung, S.H. (2007). Effects of sodium content and calcination temperature on the morphology, structure and photocatalytic activity of nanotubular titanates. *Journal of Colloid and Interface Science*, 316(2), 562–569. DOI: 10.1016/j.jcis.2007.08.008.

[11] Kalantary, R.R., Shahamat, Y.D., Farzadkia, M., Esrafili, A., Asgharnia, H. (2015). Photocatalytic Degradation and Mineralization of Diazinon in Aqueous Solution Using Nano-TiO_2 (Degussa, P25): Kinetic and Statistical Analysis. *Desalination and Water Treatment*, 55, 2. DOI: 10.1080/19443994.2014.928795.

[12] Sharma, M., Mandal, M.K., Pandey, S., Kumar, R., Dubey, K.K. (2022). Visible-Light-Driven Photocatalytic Degradation of Tetracycline using Heterostructured Cu_2O-TiO_2 Nanotubes, Kinetics, and Toxicity Evaluation of Degraded Products on Cell Lines. *ACS Omega*, 7(37), 33572–33586. DOI: 10.1021/acsomega.2c04576.

[13] Park, H., Goto, T., Han, D.H., Cho, S., Nishida, H., Sekino, T. (2020). Low Alkali Bottom-Up Synthesis of Titanate Nanotubes Using a Peroxo Titanium Complex Ion Precursor for Photocatalysis. *ACS Applied Nano Materials*, 3(8), 7795–7803. DOI: 10.1021/acsanm.0c01347.

[14] Tsai, C.-C., Teng, H. (2006). Structural Features of Nanotubes Synthesized from NaOH Treatment on TiO_2 with Different Post-Treatments. *Chemistry of Materials*, 18(2), 367–373. DOI: 10.1021/cm0518527.

[15] Zhang, X., Wang, L., Hu, W., Zheng, H., Zhang, X. (2018). The synthesis of titanium dioxide nanoparticles from titanium slag and its use for low-temperature SCR catalyst. *IOP Conference Series: Earth and Environmental Science*, 208, 012011. DOI: 10.1088/1755-1315/208/1/012011.

[16] Xu, S., Hou, Z., Chuai, X., Wang, Y. (2020). Overview of Secondary Nucleation: from Fundamentals to Application. *Industrial and Engineering Chemistry Research*, 59(41), 18335-18356. DOI: 10.1021/acs.iecr.0c03304.

[17] Yoreo, J.J. (2003). Principles of Crystal Nucleation and Growth. *Reviews in Mineralogy and Geochemistry*, 54(1), 57–93. DOI: 10.2113/0540057.

[18] Zulfiqar, M., Chowdhury, S., Omar, A.A. (2018). Hydrothermal Synthesis of Multi-walled TiO_2 Nanotubes and Its Photocatalytic Activities for Orange II Removal. *Separation Science and Technology (Philadelphia),* 53(9), 1412–1422. DOI: 10.1080/01496395.2018.1444050.

[19] Liu, N., Chen, X., Zhang, J., Schwank, J.W. (2014). A Review on TiO_2-based Nanotubes Synthesized via Hydrothermal Method: Formation Mechanism, Structure Modification, and Photocatalytic Applications. *Catalysis Today*, 225, 34-51. DOI: 10.1016/j.cattod.2013.10.090.

[20] Lee, Y., Li, Y., Zeng, H. (2013). ZnO-Based Transparent Conductive Thin Films: Doping, Performance, and Processing. *Journal of Nanomaterials,* 9, 196521. DOI: 10.1155/2013/196521.

[21] Bardestani, R., Patience, G.S., Kaliaguine, S. (2019). Experimental Methods in Chemical Engineering: Specific Surface Area and Pore Size Distribution Measurements BET, BJH, and DFT. *Canadian Journal of Chemical Engineering*, 97 (11), 2781–2791. DOI: 10.1002/cjce.23632.

[22] Morgan, D.L., Liu, H.-W., Frost, R.L., Waclawik, E.R. (2010). Implications of Precursor Chemistry on the Alkaline Hydrothermal Synthesis of Titania/Titanate Nanostructures. *The Journal of Physical Chemistry C*, 114(1), 101–110. DOI: 10.1021/jp908508z.

[23] Preda, S., Rutar, M., Umek, P., Zaharescu, M. (2015). A Study of Thermal Properties of Sodium Titanate Nanotubes Synthesized by Microwave-Assisted Hydrothermal Method. *Materials Research Bulletin*, 71, 98–105. DOI: 10.1016/j.materresbull.2015.07.015.

[24] Subramaniam, M.N., Goh, P.S., Abdullah, N., Lau, W.J., Ng, B.C., Ismail, A.F. (2017). Adsorption and Photocatalytic Degradation of Methylene Blue using High Surface Area Titanate Nanotubes (TNT) Synthesized Via Hydrothermal Method. *Journal of Nanoparticle Research*, 19 (6), 1-13. DOI: 10.1007/s11051-017-3920-9.

[25] Zhang, D., Dong, S. (2019). Progress in Natural Science: Materials International Challenges in Band Alignment between Semiconducting Materials: A Case of Rutile and Anatase TiO_2. *Progress in Natural Science: Materials International*, 29 (3), 277-284. DOI: 10.1016/j.pnsc.2019.03.012.

[26] Unal, H., Mete, E. (2014). Electronic Structures and Optical Spectra of Thin Anatase TiO_2 Nanowires Through Hybrid Density Functional and Quasiparticle Calculations. *Physical Review B,* 89 (20), 205127. DOI: 10.1103/PhysRevB.89.205127.

[27] Shah, T., Gul, T., Saeed, K. (2019). Photodegradation of Bromophenol Blue in Aqueous Medium using Graphene Nanoplates-Supported TiO_2. *Applied Water Science,* 9(4), 1–7. DOI: 10.1007/s13201-019-0983-z.

[28] Nasikhudin, N., Diantoro, M., Kusumaatmaja, A., Triyana, K. (2018). Study on Photocatalytic Properties of TiO_2 Nanoparticles in Various pH Condition. *Journal of Physics: Conference Series*, 1011, 012069. DOI: 10.1088/1742-6596/1011/1/012069.

[29] Reza, K.M., Kurny, A., Gulshan, F. (2017). Parameters Affecting The Photocatalytic Degradation of Dyes using TiO_2: A Review. *Application Water Science*, 7, 1569-1578. DOI: 10.1007/s13201-015-0367-y.